

# Rotational stacking and its electronic effects on graphene films grown on 4H-SiC(000 $\bar{1}$ )

J. Hass,<sup>1</sup> F. Varchon,<sup>2</sup> J. E. Millán-Otoya,<sup>1</sup> M. Sprinkle,<sup>1</sup> W. A. de Heer,<sup>1</sup> C. Berger,<sup>1,2</sup> P. N. First,<sup>1</sup> L. Magaud,<sup>2</sup> and E. H. Conrad<sup>1</sup>

<sup>1</sup>The Georgia Institute of Technology, Atlanta, Georgia 30332-0430, USA

<sup>2</sup>Institut Néel/CNRS-UJF BP166, 38042 Grenoble Cedex 9, France

We examine the stacking order of multilayer graphene grown on the SiC(000 $\bar{1}$ ) surface using low-energy electron diffraction and surface X-ray diffraction. We show that the films contain a high density of rotational stacking faults caused by three types of rotated graphene: sheets rotated 30° and  $\pm 2.20^\circ$  relative to the SiC substrate. These angles are unique because they correspond to commensurate phases of layered graphene, both with itself and with the SiC substrate. *Ab initio* calculations show that these rotational phases electronically decouple adjacent graphene layers. The band structure from graphene at fault boundaries displays linear energy dispersion at the  $K$ -point (Dirac cones), nearly identical to that of a single graphene sheet.

PACS numbers: 61.10.Nz, 61.14.Hg, 68.55.-a, 68.35.-p, 73.20.At, 71.15.Mb

Keywords: Graphene, Graphite, LEED, X-ray diffraction, SiC, Silicon carbide, *ab initio* calculations

In the last few years an intriguing series of experiments suggests that a new all-carbon paradigm for electronic circuits may be possible [1, 2, 3, 4]. In this system graphene sheets are lithographically cut into ribbons to produce gates and wires from a single material [1, 5, 6]. The promise of this new approach to electronics rests on the ability to make large single or multilayer graphene sheets on a substrate that preserves the electronic properties of an isolated graphene sheet.

Both exfoliated graphene flakes [2, 3] and multilayer graphene grown on SiC [7, 8] exhibit 2D transport properties characteristic of chiral Dirac electrons expected for an isolated graphene sheet. These include a Berry phase of  $\pi$  in the integer quantum Hall effect and suppressed back-scattering [2, 4, 9]. SiC-grown films offer the most practical and scalable approach to 2D graphene electronics, but the effect of the substrate and graphene stacking must be clarified. Recent X-ray diffraction measurements and electronic structure calculations showed that the graphene-SiC(000 $\bar{1}$ ) substrate interaction is weak, except for a strongly-bound (non-conducting) buffer layer isolating subsequent graphene layers from the SiC [10, 11]. However, the remaining paradox is that normal *AB*...stacked (Bernal) graphite breaks the equivalency of *A* and *B* atoms in a graphene sheet [12, 13] so that multilayer films should not exhibit the graphene-like properties that are clearly observed on 4H-SiC(000 $\bar{1}$ ) substrates [4, 14]. As we will show, in this case nature provides a new stacking sequence that preserves the electronic symmetry of graphene.

In this Letter we present Low Energy Electron Diffraction (LEED) and surface X-ray scattering data for multilayer graphene grown on the 4H-SiC(000 $\bar{1}$ ) carbon-terminated surface (C-face). We show that graphene grows in three forms on this surface: layers rotated 30°

( $R30$ ), or  $\pm 2.20^\circ$  ( $R2^\pm$ ) from the SiC bulk [10 $\bar{1}0$ ] direction. In contrast, 4H-SiC(0001) (Si-face) films orient only in the  $R30$  phase (known as the  $(6\sqrt{3} \times 6\sqrt{3})R30^\circ$  reconstruction in SiC coordinates) [7]. X-ray diffraction on C-face films confirms that all three rotated phases occur, causing a high density of rotational fault boundaries between  $R30$  and  $R2^\pm$  layers. *Ab initio* electronic calculations for this type of stacking show that adjacent rotated planes become electronically decoupled, preserving the Dirac dispersion at the  $K$ -point. These results explain how, even in multilayer graphene, the films maintain the electronic properties of an isolated graphene sheet.

All substrates were 4H-SiC(000 $\bar{1}$ ) prepared as previously reported [8]. Once samples are graphitized, they remain relatively inert, allowing them to be transported into the vacuum chamber. The X-ray scattering experiments were performed at the Advanced Photon Source, Argonne National Laboratory, on the 6IDB and C- $\mu$ CAT beam lines at 16.2 keV photon energy. Samples were mounted in a vacuum cryostat in the diffractometer. Reciprocal space points are reported in the reciprocal lattice units (*r.l.u.*) of the standard graphite hexagonal reciprocal lattice,  $\mathbf{q} = (h\mathbf{a}^*, k\mathbf{b}^*, l\mathbf{c}^*)$ , where  $|\mathbf{a}^*| = |\mathbf{b}^*| = 2\pi/(a\sqrt{3}/2)$  and  $|\mathbf{c}^*| = 2\pi/c$ . The nominal lattice constants for graphite are  $a = 2.4589\text{\AA}$ ,  $c = 6.674\text{\AA}$  [15].

While it is known that graphene grows epitaxially only in the  $R30$  phase on the 4H-SiC(0001) Si-face, multilayer graphene grown on the C-face was thought to have a high degree of azimuthal disorder because of streaking in LEED images [7]. However, a detailed look at the diffraction shows that the rotational disorder is not random. This is demonstrated in the LEED image from a film with  $\sim 10$  graphene layers [Fig. 1(a)]. The pattern has two characteristics; (i) an oriented  $R30$  film evidenced by graphene spots (rods) rotated  $\pm 30^\circ$  from the SiC [10 $\bar{1}0$ ]

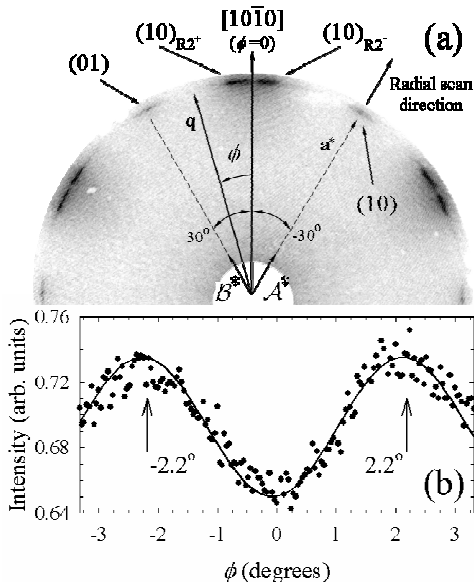


FIG. 1: (a) A LEED image acquired at 67.9eV from 4H-SiC(000 $\bar{1}$ ) C-face with  $\sim 10$  graphene layers showing only graphite spots and diffuse rings. The SiC  $[10\bar{1}0]$  direction is marked for reference. The SiC  $(6\sqrt{3} \times 6\sqrt{3})R30^\circ$  unit vectors  $\mathcal{A}^*$  and  $\mathcal{B}^*$  are shown for reference. (b) X-ray azimuthal scans of the diffuse graphite ring around  $\phi = 0.0$  and  $|q| = |a^*|$ .

direction and (ii) azimuthally diffuse rings centered at  $0^\circ$  from the SiC  $[10\bar{1}0]$  direction. Note that the diffuse rings are not continuous but split. This is seen more clearly in Fig. 1(b) that shows an X-ray azimuthal scan ( $\phi$  scan) taken at the radial position of the graphite rod ( $|q| = a^*$ ) in Fig. 1(a)) around  $\phi = 0.0^\circ$ . The scan shows diffuse intensity that is peaked at  $\phi = \pm 2.2^\circ$ .

The significance of the  $\pm 2.2^\circ$  preferred rotation is two-fold. First, graphene is nearly commensurate with the SiC substrate on a length scale equal to a  $(13 \times 13)$  graphene unit cell (rotated  $30^\circ$  from SiC). The  $(13 \times 13)$  cell is  $\sim 0.14\%$  smaller than the SiC  $(6\sqrt{3} \times 6\sqrt{3})R30^\circ$  cell. What has not been recognized is that there are two additional ways to orient a  $(13 \times 13)$  graphene sheet that give rise to a film commensurate with the SiC  $(6\sqrt{3} \times 6\sqrt{3})R30^\circ$  structure. They can be calculated when the magnitude of the SiC  $(6\sqrt{3} \times 6\sqrt{3})$  reciprocal lattice vector is nearly equal to the graphene reciprocal lattice;

$$|n\mathcal{A}^* + m\mathcal{B}^*| \approx |a^*|. \quad (1)$$

$n$  and  $m$  are integers.  $\mathcal{A}^*$  and  $\mathcal{B}^*$  are the reciprocal lattice vectors of the  $(6\sqrt{3} \times 6\sqrt{3})R30^\circ$  structure (see Fig. 1(a)),  $|\mathcal{A}^*| = |\mathcal{B}^*| = |a_{\text{SiC}}^*|/(6\sqrt{3})$  with  $a_{\text{SiC}}^* = 2.3554\text{\AA}^{-1}$ . The rotation angle of the commensurate graphene relative to SiC can be calculated for different  $m$  and  $n$ 's:

$$\cos \phi = \frac{\sqrt{3}}{2} \frac{n+m}{\sqrt{n^2+m^2+nm}}. \quad (2)$$

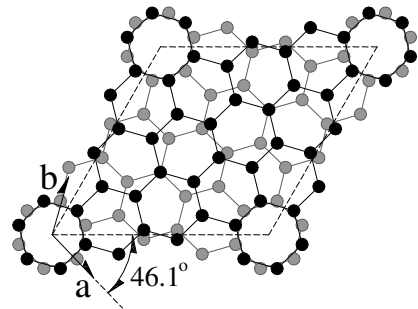


FIG. 2: Schematic  $(\sqrt{13} \times \sqrt{13})R46.1^\circ$  fault pair unit cell (dashed line). Dark circles are  $R30$  graphene atoms ( $\mathbf{a}$  and  $\mathbf{b}$  are graphene unit vectors). Gray circles are graphene atoms in the  $R2^+$  plane below, rotated  $32.204^\circ$  from the top plane.

Equation (1) is satisfied when  $(n, m) = (13, 0)$ ,  $(8, 7)$  or  $(7, 8)$ . All three solutions give the SiC  $(6\sqrt{3} \times 6\sqrt{3})R30^\circ$  cell but the first solution has graphene rotated  $30^\circ$  relative to SiC while the other two solutions have graphene rotated  $\pm 2.204^\circ$  relative to SiC. Graphene grown on the Si-face of SiC only locks into the  $30^\circ$  structure. However, as the diffraction in Fig. 1(a) clearly shows, all three phases appear on C-face grown multilayer graphene. For future discussion we will index the two spots near  $\phi = 0$  as the  $(1, 0, \ell)_{R2^+}$  and  $(1, 0, \ell)_{R2^-}$  graphene rods. It is worth noting that, aside from the  $(1, 0, \ell)_{R2^\pm}$  rods, other  $(6\sqrt{3} \times 6\sqrt{3})R30^\circ$  reconstruction spots must be weak since they are not seen in LEED. This is in contrast to Si-face grown graphene where the additional spots indicate a complicated interfacial graphene reconstruction. Apparently C-face graphene has a weaker substrate interaction compared to Si-face graphene that may explain why the additional rotated phases are specific to C-face films.

The significance of these three phases is even more important if we recognize that two graphene sheets can be rotated relative to each other in a number of ways that make the two sheets commensurate with each other [16]. The lowest energy commensurate rotation angles are precisely  $\phi = \cos^{-1}(11/13)$  or  $\cos^{-1}(-11/13) - 120^\circ$  i.e.,  $30 \pm 2.204^\circ$  [16]. This bi-layer commensurate structure corresponds to a graphene  $(\sqrt{13} \times \sqrt{13})R(\pm 46.1^\circ)$  cell that costs 3–5meV/atom more than  $AB \dots$  stacking [a schematic of a fault pair is shown in Fig. 2] [16].

While the observation of three rotational phases is interesting, it is the stacking of these rotated planes that bears directly on their electronic properties. The  $R30$  and  $R2^\pm$  phases do not exist as isolated domains. Instead all three rotations are present in a multilayer graphene stack and lead to a high density of  $R30/R2^\pm$  fault pairs. The most direct evidence for this comes from high-resolution X-ray diffraction. Figure 3(a) shows X-ray radial scans [see Fig. 1(a)] through the graphite  $(1, 0, \ell)$  rod for different values of  $\ell$ . The two non-dispersing peaks correspond to a normal graphene  $(1, 0, \ell)$  surface

rod and the other to a surface rod  $(1 + \Delta h, 0, \ell)$  from graphene with a compressed in-plane lattice constant. The peak separation corresponds to a lattice compression of  $\Delta a/a = \Delta h/(1 + \Delta h) = -0.28 \pm 0.01\%$ . Note that the compressed and uncompressed rods widths are the same, meaning that the ordered size of these two types of graphene sheets are similar. It is important to realize that the compressed lattice is not a result of epitaxial strain between the graphene and the SiC substrate, which would increase the graphene in-plane lattice constant.

We can identify the compressed graphene as those sheets at the  $R30/R2^\pm$  fault boundary shown in Fig. 2. This conclusion is derived from two key pieces of information found in the intensity modulation of the  $(1, 0, \ell)$  rod [see Fig. 3(b)]. First, in normal graphite, the primary fault type is rhombohedral  $ABC\dots$  stacking. Faults of this type would produce a peak in the  $(1, 0, \ell)$  at  $\ell = 1.5$  that is clearly not seen in the data in Fig. 3(b).

Second,  $AA\dots$  and  $ABC\dots$  faults are expected to cause small inter-layer *contractions*  $\sim 0.2\%$  [17]. Instead, our X-ray results show a large interplanar *expansion* at the fault boundary. This is shown in the inset of Fig. 3(b) where the experimental peak at  $\ell = 2$  is shifted to a slightly lower value. This indicates a larger inter-layer spacing than bulk graphite. We can estimate the interplanar expansion at the fault using a model where random rotational faults are introduced with a probability  $\gamma$ , and each  $R30/R2^\pm$  boundary expands by  $\epsilon$ . A fit with  $\gamma = 0.38$  and  $\epsilon = 0.06\text{\AA}$  is shown in Fig. 3(b). This large expansion (1.8%) is characteristic of azimuthally disordered turbostratic graphite with many rotational faults that cause significant interference of  $\pi^*$  states between rotated planes [15]. Note that this large interlayer expansion is also consistent with the in-plane contraction of the fault. Graphite's thermal expansion is negative in-plane and positive out-of-plane [18]. A weaker inter-layer bond caused by the large expansion at the fault allows the in-plane bonds to contract [18, 19].

We expect significant changes in the electronic properties of the graphene films when the rotated stacking fault density is as high as we observe. For a  $R30/R2^\pm$  fault pair there are only 2 atoms/sheet out of 52 in the  $(\sqrt{13} \times \sqrt{13})R(\pm 46.1^\circ)$  cell that are in high symmetry positions. This suggests weak interplanar interactions in the fault pairs. To understand how the rotational stacking affects the electronic properties of these films, we have performed an *ab initio* Density Functional Theory (DFT) band structure calculation for a  $R30/R2^\pm$  free standing graphene fault pair. The calculations are performed using the VASP [20] code within the generalized gradient approximation [21]. Ultra soft pseudopotentials [22] are used with a plane wave basis cutoff equal to 211 eV. All calculations are performed on the same bi-layer commensurate cell, the  $(\sqrt{13} \times \sqrt{13})R(\pm 46.1^\circ)$ . This cell contains two graphene sheets of 26 carbon atoms each, rotated  $32.204^\circ$  relative to each other [see Fig. 2]. The empty

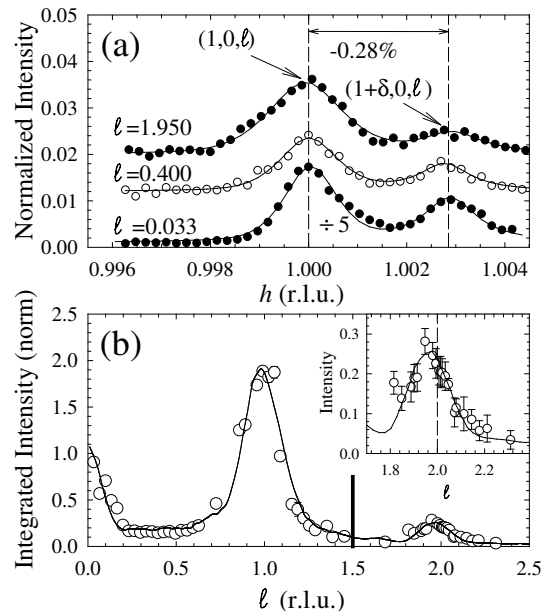


FIG. 3: (a) Radial ( $h$ ) scans through the graphite ( $h = 1, 0, \ell$ ) rod for different  $\ell$  (see Fig. 1). Scans show two peaks corresponding to the normal graphene  $(1, 0, \ell)$  rod and a compressed graphene  $(1 + \Delta h, 0, \ell)$  rod. (b) Integrated intensity of the  $(1, 0, \ell)$  rod. Solid line is a fit to a random rotational fault model. Vertical bar marks the expected position of a peak from  $ABC\dots$  faults. Inset is an expanded view near  $\ell = 2$  showing a shift to smaller  $\ell$  (larger inter-layer spacing).

space width is equal to  $24\text{\AA}$ . The total energy of the rotated stacking cell is  $1.6\text{meV/atom}$  higher than an  $AB\dots$  cell. This energy difference is slightly smaller than other estimates of this structure [16].

For bilayers, the interlayer distance is fixed to  $3.39\text{\AA}$ . As a check, we have varied this distance and found no qualitative change in the band structure results. This check was performed since DFT is known to poorly describe van der Waals forces and gives rise to theoretical graphene interlayer spacings significantly larger than experimental values. However, we point out that the C-short ultrasoft pseudopotential used here has been extensively tested [10, 23] and was shown to correctly describe the band structure of graphite. Integration over the Brillouin zone is performed on a  $30 \times 30 \times 1$  grid in the Monkhorst-Pack scheme to ensure convergence of the Kohn-Sham eigenvalues. Due to the faulted cell symmetry, the  $K$ -points of the graphene  $1 \times 1$  cell for the 2 layers of the rotated stacking are translated to the  $K$ -point of the  $(\sqrt{13} \times \sqrt{13})R(\pm 46.1^\circ)$  Brillouin zone.

The results of this calculation are shown in Fig. 4 where we compare the band structure for an isolated graphene sheet, a graphene bi-layer with Bernal  $AB\dots$  stacking, and a bilayer rotation fault pair with the  $(\sqrt{13} \times \sqrt{13})R(\pm 46.1^\circ)$  structure (the  $\Gamma K M$  direction shown is the  $(\sqrt{13} \times \sqrt{13})R \pm 46.1^\circ$  cell high symmetry di-

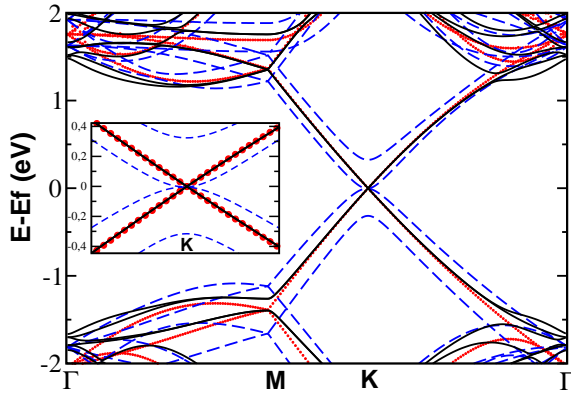


FIG. 4: Calculated band structure for three forms of graphene. (i) isolated graphene sheet (solid line), (ii)  $AB\dots$  graphene bilayer (dashed line), and (iii)  $R30/R2^+$  fault pair (dots). Inset shows details of band structure at the  $K$ -point showing no difference between the Dirac cone for an  $R30/R2^+$  fault pair and a single graphene layer.

rection). The main differences in the electronic structure among the three forms of graphene shows up in the dispersion curves in the vicinity of the  $K$ -points. The band structure for an isolated graphene sheet shows the known linear gapless dispersion (Dirac cone) of the  $\pi$  bands at the  $K$ -point. The normal Bernal  $AB\dots$  stacking of graphene breaks the sublattice symmetry, giving rise to splitting of the  $\pi$  bands with a corresponding change to a parabolic shape and a lower group velocity [13]. With the rotated fault, the linear dispersion is recovered in the vicinity of the  $K$ -points. This dispersion is identical to the graphene dispersion (same Fermi velocity) and clearly shows that in the rotated layers, the atoms in the  $A$  and  $B$  sublattices are identical. This result also holds for infinite stacks: a graphite-like system made of graphene sheets rotated alternately by  $0^\circ$  and  $30 \pm 2.204^\circ$  also shows a linear dispersion near the  $K$ -point. This result is similar to the continuum description of Santos et. al [24] for two graphene sheets rotated by much smaller relative angles.

In conclusion, we have shown that multilayer graphene grown on the carbon terminated face of 4H-SiC does not grow as a simple  $AB\dots$  stacked film. Instead the graphene-SiC and graphene-graphene commensurations produce a high density of rotational faults where adjacent sheets are rotated  $30^\circ \pm 2.204^\circ$  relative to each other. These rotational faults cause adjacent graphene sheets to decouple electronically. The result is that the band structure of faulted sheets is nearly identical to isolated graphene. Specifically, the Dirac dispersion at the  $K$ -point is preserved even though the film is composed of many graphene sheets. This may explain why magnetotransport [4] and infrared magnetotransmission [14] experiments on similar samples give results very similar to those of an isolated graphene sheet.

We wish to acknowledge N. Wipf, G. Trambly de Laisardière and D. Mayou for fruitful discussions about the energetics of rotated graphene. This research was supported by the National Science Foundation under Grant No. 0404084 and by Intel Research. The Advanced Photon Source is supported by the DOE Office of Basic Energy Sciences, contract W-31-109-Eng-38. The  $\mu$ -CAT beam line is supported through Ames Lab, operated for the US DOE under Contract No. W-7405-Eng-82.

- 
- [1] C. Berger, Z. Song, T. Li, X. Li, A.Y. Ogbazghi, R. Feng, Z. Dai, T. Grenet, A.N. Marchenkov, E.H. Conrad, P.N. First, W.A. de Heer, *J. Phys. Chem.* **B 108**, 19912 (2004).
  - [2] K.S. Novoselov, A.K. Geim, S.V. Morozov, D. Jiang, M.I. Katsnelson, I.V. Grigorieva, S.V. Dubonos and A.A. Firsov, *Nature* **438**, 197 (2005).
  - [3] Y. Zhang, Y.-W. Tan, H.L. Stormer and P. Kim, *Nature* **438**, 201 (2005).
  - [4] C. Berger, Z. Song, X. Li, X. Wu, N. Brown, C. Naud, D. Mayou, T. Li, J. Hass, A.N. Marchenkov, E.H. Conrad, P.N. First and W.A. de Heer, *Science* **312**, 1191 (2006).
  - [5] K. Nakada, M. Fujita, G. Dresselhaus, and M.S. Dresselhaus, *Phys. Rev.* **B54** 17954 (1996).
  - [6] K. Wakabayashi, M. Fujita, H. Ajiki, M. Sigrist, *Phys. Rev.* **B59**, 8271 (1999).
  - [7] I. Forbeaux, J.-M. Themlin, A. Charrier, F. Thibaudau, and J.-M. Debever, *Appl. Surf. Sci.* **162/163**, 406 (2000).
  - [8] J. Hass, R. Feng, T. Li, X. Li, Z. Song, W.A. de Heer, P.N. First, E.H. Conrad, C.A. Jeffrey, and C. Berger, *Appl. Phys. Lett.* **89**, 143106 (2006).
  - [9] X. Wu and X. Li and Z. Song and C. Berger and W.A. de Heer, *Phys. Rev. Lett.* **98**, 136801 (2007).
  - [10] F. Varchon, R. Feng, J. Hass, X. Li, B. Ngoc Nguyen, C. Naud, P. Mallet, J.-Y. Veuillen, C. Berger, E.H. Conrad and L. Magaud, [arxiv.org/abs/cond-mat/0702311](http://arxiv.org/abs/cond-mat/0702311) (2007).
  - [11] J. Hass, R. Feng, J.E. Millán-Otoya, X. Li, M. Sprinkle, P. N. First, C. Berger, W. A. de Heer and E. H. Conrad, *Phys. Rev. B*, (in press) (2007).
  - [12] E. McCann and V. I. Fal'ko, *Phys. Rev. Lett.* **96** 086805 (1996).
  - [13] S. Latil and L. Henrard, *Phys. Rev. Lett.* **97**, 036803 (2006).
  - [14] M. L. Sadowski and G. Martinez and M. Potemski and C. Berger and W.A. de Heer, *Phys. Rev. Lett.* **97**, 266405 (2006).
  - [15] J. Baskin and L. Mayer, *Phys. Rev.* **100** 544 (1955).
  - [16] A.N. Kolmogorov, and V.H. Crespi, *Phys. Rev.* **B71** 235415 (2005).
  - [17] J.-C. Charlier, X. Gonze, and J.-P. Michenaud, *Carbon*, Vol. **32**, (Elsevier, Great Britain, 1994) p. 289.
  - [18] G.D. Barrera, J.A.O. Bruno, T.H.K. Barron and N.L. Allan, *J. Phys. Condens. Matter* **17** R217 (2005).
  - [19] M. Weinert, E. Wimmer, and A.J. Freeman, *Phys. Rev.* **B26** 4571 (1982).
  - [20] G. Kresse and J. Hafner, *Phys. Rev.* **B47**, 558 (1993).
  - [21] J. P. Perdew and Y. Wang, *Phys. Rev.* **B33**, 8800 (1986).

- [22] G. Kresse and J. Hafner, *J. Phys. Condens. Matter* **6**, 8245 (1994).
- [23] A. Incze, A. Pasturel, P. Peyla, *Phys.Rev.* **B66**, 172101 (2002); A.Incze, PhD thesis (2002), Grenoble, France.
- [24] J.M.B. Lopes dos Santos, N.M.R. Peres, A.H. Castro Neto, arXiv:0704.2128v1 [cond-mat.mtrl-sci].